Structural and Multidisciplinary Optimization manuscript No.
(will be inserted by the editor)

On the optimality of Hemp's arch with vertical hangers

Aleksey V. Pichugin · Andrew Tyas · Matthew Gilbert

Received: ??? / Accepted: ???

Abstract In 1974 W. S. Hemp constructed a prototype structure to carry a uniformly distributed load between two pinned supports. Although Hemp's structure had a significantly lower volume than a parabolic arch with vertical hangers, it was shown to fail the Michell optimality criteria, and therefore to be non-optimal. In this paper we demonstrate that if limiting compressive and tensile stresses are *unequal* then Hemp's structure is optimal for the half-plane provided the ratio of limiting tensile to compressive stresses falls below a certain threshold. An analytical proof is presented and the finding is confirmed by results from large scale numerical layout optimization simulations.

Keywords truss optimization, Michell structure, uniformly distributed load.

1 Introduction

Optimum structures capable of carrying distributed loads are of obvious interest to structural engineers. For certain classes of structures, optimum solutions can be readily deduced for a wide range of distributed load and support configurations. So-called "Prager structures" or "optimal arch-grids" are one such class of structures which has been characterized by Rozvany and Prager (1979). All non-zero member forces within a Prager structure must be of the same sign and, in addition, the vertical positions of external loads must be chosen optimally. Rozvany and Wang (1983) show that these two conditions ensure that Prager structures are always funicular in form. Current understanding of more complex classes of optimum structures, which satisfy the Michell optimality criteria, is more limited (Michell (1904); Hemp (1973); Rozvany et al (1995)). Whilst elementary examples of Michell trusses capable of supporting distributed loads can be obtained using the principle of superposition, the fact that relatively few Michell structures are known, coupled with the limited validity of the superposition principle itself, limits the applicability of the approach.

Details of the first non-trivial example of a Michell-like structure capable of carrying a distributed load were provided by Hemp (1974). The structure proposed in Hemp's paper transfers a uniformly distributed load to two level pinned supports. The volume of the resulting structure is some 3.5% lower than that of a simple parabolic arch with vertical hangers. The semi-inverse method developed by Hemp to characterize his structure proved equally effective when analysing a closely related optimum structure, designed to carry a uniform *transmissible* load between two pinned supports (Tyas et al 2011). However, when Hemp analysed the virtual displacement field corresponding to his structure, it transpired that the Michell optimality criteria were violated in a small area near mid-span, indicating that his solution was not optimal. Chan (1975) partially resolved this difficulty by showing that Hemp's structure was, in fact, optimal for certain non-uniformly distributed patterns of loading. The present paper is in a sense complementary to Chan's, but here it is demonstrated that Hemp's structure can be optimal for a uniformly distributed load after all, provided the limiting compressive stress is sufficiently large in comparison to the limiting tensile stress.

The structure proposed by Hemp comprises of two regions; Fig. 1 shows the left half-span. The first region is a fan of fully strained mutually orthogonal bars. The uppermost

Aleksey V. Pichugin
Department of Mathematical Sciences
Brunel University, Uxbridge, UB8 3PH, UK
E-mail: aleksey.pichugin@brunel.ac.uk

Andrew Tyas · Matthew Gilbert
Department of Civil and Structural Engineering
University of Sheffield, Sheffield, S1 3JD, UK
E-mail: a.tyas@sheffield.ac.uk
E-mail: m.gilbert@sheffield.ac.uk

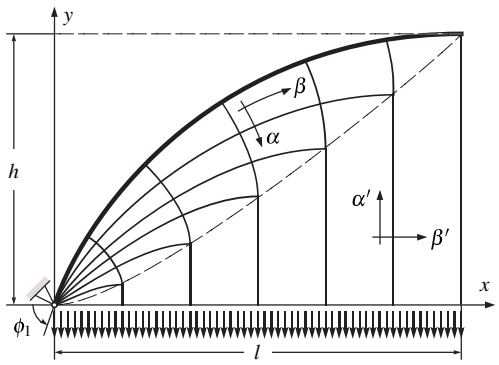

Fig. 1 Half-span of the structure proposed by Hemp (1974).

bar in the fan is a concentrated element which equilibrates the horizontal thrust at mid-span. At the bottom boundary of the fan the constituent bars are aligned with the Cartesian axes; the horizontal components of the bar forces reduce to zero on this boundary whilst the vertical components of the bar forces are equilibrated by vertical hangers, which transfer the distributed applied load to the bottom of the fan.

The present study was partly motivated by the recent availability of high resolution numerical data corresponding to Hemp's problem in its original formulation. Fig. 2 shows a solution obtained using layout optimization software which incorporates the highly efficient adaptive 'member-adding' procedure developed by the authors (Gilbert and Tyas 2003). Evidently, the sections of the structure in the vicinity of supports appear to follow Hemp's proposed solution quite accurately. Nevertheless, at some point the vertical hanger bars become inclined and, in order to equilibrate the horizontal component of the bar forces, a further concentrated tie bar emerges along the bottom boundary. This finding coincides with that derived from early numerical analyses by McConnel (1974), and the concentrated tie bar along the bottom boundary is also evident in numerical output obtained more recently by Gilbert et al (2005). It is worth remarking that another non-trivial example of a structure with a functionally similar horizontal tie bar is given by Sokół and Lewiński (2010), who also draw on numerical layout optimization techniques to confirm their analytical results (Sokół 2011).

The presence of the horizontal tie bar allows some important observations about the nature of the true optimal solution to be drawn:

- It is evident that the inclined tie bars are not orthogonal to the concentrated tie bar at the bottom of the structure. This is therefore an example of a degenerate Maxwell-type region, where strains are at their (tensile) limit in all directions. Such regions do not impose any restrictions on member layout. Rozvany (1997) describes several other situations when the usual assumptions of member orthogonality within Michell structures can be relaxed. Note that an analytical solution for a structure featuring a similar concentrated tie bar, which transmits a uniform vertical load along a family of inclined tie bars, has recently been presented by the authors (Pichugin et al, 2011).
- The curvature of the concentrated compressive member at the crown cannot be accurately reproduced using the rectangular nodal grid employed. This leads to gaps within the structure, which can be seen to be comparatively wide around mid-span. Consequently it is not possible to accurately determine whether or not the fans of mutually orthogonal members meet at mid-span.
- The inclined bars must follow the trajectories of tensile members at the bottom boundary of the fan of mutually-orthogonal fully-strained members. This violates Hemp's assumption that members along the bottom boundary of the fan must be aligned with the Cartesian axes. This indicates that the regions of mutually orthogonal members connected to the inclined tie bars cannot possibly be identical to the Hencky-type fans constructed by Hemp (1974).

The availability of efficient layout optimization software also allowed the dependence of the optimal solution on the ratio of limiting tensile and compressive stresses to be studied. The ensuing computations indicated the length of the mid-span horizontal tensile member to be strongly dependant on this ratio. It was also observed that the extent of the section of the structure comprising vertical ties in Fig. 2 extends to cover the whole span when the ratio of limiting tensile to compressive stresses is sufficiently small, with the mid-span horizontal tensile member then disappearing completely. This implied that the structure comprising vertical ties originally proposed by Hemp could potentially be optimal in some circumstances. The remainder of the paper is devoted to proving this hypothesis, and to identifying the critical ratio of limiting stresses for which Hemp's structure becomes optimal.

2 Some results from Hemp's 1974 paper

In the interests of conciseness several useful formulae taken from Hemp (1974) are presented without derivation in this section. The notation, where possible, is also the same as used in Hemp's article. At the same time, to clarify the relationship between our and Hemp's derivations, we will specify the numbers of relevant equations in Hemp's paper; these will be given in square brackets to distinguish them from the equations in the present paper.

The fan can be conveniently parametrized by a curvilinear orthogonal coordinate system (α,β), see Fig. 1. If β denotes the angle ϕ from Ox to the local tangent to an α

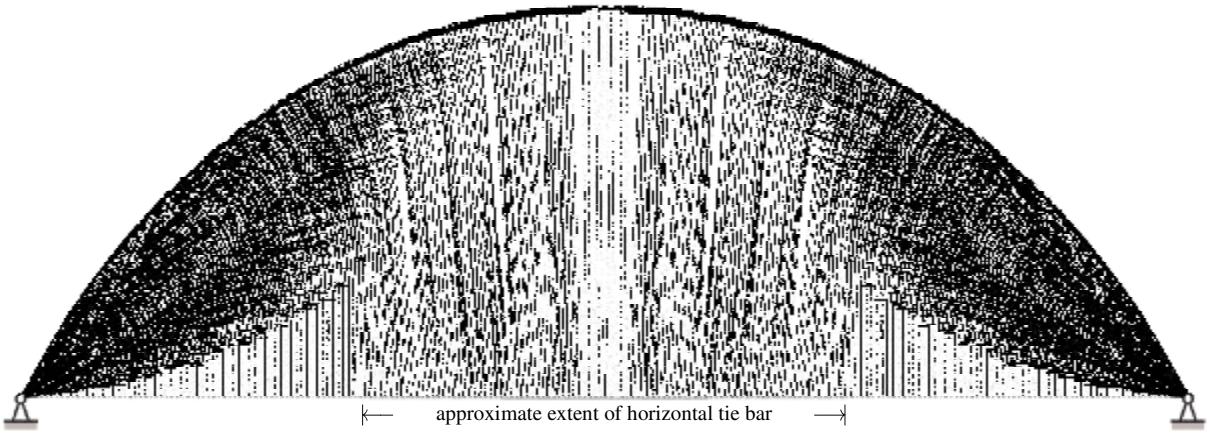

Fig. 2 Full span of the optimum structure in the case of equal limiting stresses in compression and tension. This numerical solution was obtained using a uniform Cartesian grid comprising 181×253 nodal points, and involved considering approx. 1.048×10^9 potential members.

line (increasing) and ϕ_1 is the angle of the fan at the support, then $0 \leqslant \beta \leqslant \phi_1$ and

$$\phi = -\pi/2 + \phi_1 - \alpha - \beta\,. \tag{1}$$

Within this coordinate system, line $\alpha = 0$ corresponds to the top boundary of the fan and line $\alpha = \phi_1 - \beta$ (i.e. $\phi = -\pi/2$) corresponds to its bottom boundary. Fan angle ϕ_1, presently unknown, is best thought of as a tuning parameter, which can be used to ensure the compatibility of the static and kinematic fields.

The static solution and the geometry of the fan, characterized in the first two sections of Hemp's paper, are fully applicable in our case. In particular, the Lamé coefficients (i.e. the scale factors for the chosen system of orthogonal curvilinear coordinates) are given at the bottom of the fan by the following expressions

$$A(\phi_1-\beta,\beta) = \frac{l^2}{2h}\int_0^\beta \frac{I_1(2\phi_1-2\xi)I_1(2\beta-2\xi)}{(\beta-\xi)(\phi_1-\xi)}\mathrm{d}\xi\,, \tag{2}$$

$$B(\phi_1-\beta,\beta) = \frac{l^2}{2h}\frac{I_1(2\phi_1-2\beta)}{\phi_1-\beta}\,, \tag{3}$$

cf. equations [23] and [12], respectively. Within (2) and (3) l and h denote the half-span and the height of the structure, see Fig. 1, and $I_n(x)$, $n = 0, 1, \ldots$, stand for modified Bessel functions of the first kind. The general theory of Michell fields featuring mutually orthogonal members can then be used to establish the Cartesian coordinates of the bottom of the fan:

$$x(\phi_1-\beta,\beta) = \int_0^\beta B(\phi_1-\zeta,\zeta)\mathrm{d}\zeta\,, \tag{4}$$

$$y(\phi_1-\beta,\beta) = \int_0^\beta A(\phi_1-\zeta,\zeta)\mathrm{d}\zeta\,. \tag{5}$$

Since $x(0,\phi_1) = l$, integral (5) can be evaluated at the top of the fan, yielding

$$\begin{aligned}\frac{h}{l} &= \int_0^{\phi_1}\frac{I_1(2\phi_1-2\zeta)}{2(\phi_1-\zeta)}\mathrm{d}\zeta = \int_0^{2\phi_1}\frac{I_1(\xi)}{2\xi}\mathrm{d}\xi \\ &= \tfrac{1}{2}I_1(2\phi_1) + \sum_{n=1}^{\infty}(-1)^n I_{2n+1}(2\phi_1) \equiv H_1(\phi_1)\,,\end{aligned} \tag{6}$$

cf. equations [26, 27].

3 The case of unequal limiting stresses

3.1 Virtual displacement field within the fan

It is now necessary to derive a virtual displacement field which is valid for unequal limiting compressive and tensile stresses, denoted σ_C and σ_T, respectively. The strains produced by this field must satisfy the requirements of the Michell criteria, i.e. remain bounded by the maximum allowable values $-\ell\sigma/\sigma_C$ and $\ell\sigma/\sigma_T$, in which $\sigma = (\sigma_C + \sigma_T)/2$ and ℓ is a positive infinitesimal. It is shown in Hemp (1973) that within regions of mutually orthogonal members, such as within the fan region, the rotation is given by

$$\omega = \omega_0 - \ell\sigma\left(\frac{1}{\sigma_C}+\frac{1}{\sigma_T}\right)(\alpha-\beta)\,. \tag{7}$$

The reflection symmetry of the structure requires that the rotation must vanish at the top of the fan, hence $\omega_0 = -\ell\sigma(1/\sigma_C + 1/\sigma_T)\phi_1$. The implication is that at the bottom of the fan one has

$$\omega = -2\ell\sigma\left(\frac{1}{\sigma_C}+\frac{1}{\sigma_T}\right)(\phi_1-\beta)\,, \tag{8}$$

which generalizes [29]. With the rotation known one can use the standard expressions for virtual displacements (Hemp,

1973, p. 75) to find that at the bottom of the fan

$$u(\phi_1-\beta,\beta) = -\int_0^\beta \left[\frac{\ell\sigma}{\sigma_T}A(\phi_1-\zeta,\zeta)+\omega B(\phi_1-\zeta,\zeta)\right]\mathrm{d}\zeta\,, \quad (9)$$

$$v(\phi_1-\beta,\beta) = -\int_0^\beta \left[\frac{\ell\sigma}{\sigma_C}B(\phi_1-\zeta,\zeta)+\omega A(\phi_1-\zeta,\zeta)\right]\mathrm{d}\zeta\,, \quad (10)$$

where u and v denote displacements in directions of increasing α and β respectively. Using (2), (3) and (5), integral (9) can be evaluated explicitly. The resulting expression

$$u(\phi_1-\beta,\beta) = -\ell\sigma y(\phi_1-\beta,\beta)/\sigma_T + \frac{\ell\sigma l^2}{2h}\left(\frac{1}{\sigma_C}+\frac{1}{\sigma_T}\right)(I_0(2\phi_1)-I_0(2\phi_1-2\beta)) \quad (11)$$

generalizes [33]. Integral (10) is more complicated. Using (3) and (4), it can be re-written as

$$v(\phi_1-\beta,\beta) = -\ell\sigma x(\phi_1-\beta,\beta)/\sigma_C + 2\ell\sigma\left(\frac{1}{\sigma_C}+\frac{1}{\sigma_T}\right)\int_0^\beta(\phi_1-\zeta)A(\phi_1-\zeta,\zeta)\mathrm{d}\zeta\,. \quad (12)$$

At the top of the fan v becomes equal to the horizontal displacement, which must vanish due to the symmetry of the structure. Therefore, in view of definition (2), equation (12) implies that

$$h/l = (1+\sigma_C/\sigma_T)H_0(\phi_1)\,, \quad (13)$$

where

$$H_0(\phi_1) = \int_0^{\phi_1}(\phi_1-\zeta)\int_0^\zeta \frac{I_1(2\phi_1-2\xi)I_1(2\zeta-2\xi)}{(\phi_1-\xi)(\zeta-\xi)}\mathrm{d}\xi\mathrm{d}\zeta\,. \quad (14)$$

In Appendix 3 of his paper, Hemp demonstrated that

$$H_0(\phi_1) = [I_0(2\phi_1)+1]H_1(\phi_1)-H_2(\phi_1)\,, \quad (15)$$

within which

$$H_2(\phi_1) = \int_0^{2\phi_1}\frac{I_0(\xi)I_1(\xi)}{\xi}\mathrm{d}\xi = 2\phi_1[I_0^2(2\phi_1)-I_1^2(2\phi_1)]-I_0(2\phi_1)I_1(2\phi_1)\,. \quad (16)$$

The combination of (6) and (13)–(16) yields the secular equation for ϕ_1:

$$H_1(\phi_1) = \frac{2\phi_1[I_0^2(2\phi_1)-I_1^2(2\phi_1)]-I_0(2\phi_1)I_1(2\phi_1)}{I_0(2\phi_1)+\dfrac{\sigma_C}{\sigma_T+\sigma_C}}\,, \quad (17)$$

generalising [37]. Equation (17) must be solved numerically. For example, in the case of equal limiting stresses it is found that $\phi_1\approx 1.10176$ and, from (6), $h/l\approx 0.676885$. Numerical solutions were also computed for the full range of $0<\sigma_T/\sigma_C\leqslant 1$. The results of these computations are presented in Fig. 3. Evidently, both ϕ_1 and h/l, see (6), increase (or decrease) together with σ_T/σ_C.

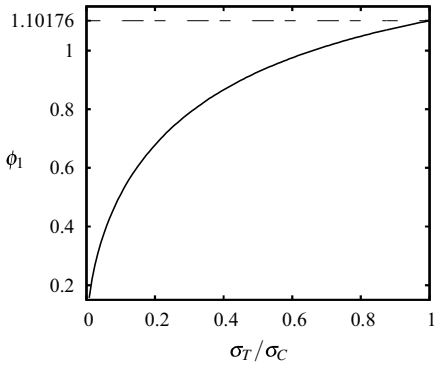

Fig. 3 Dependence of fan angle ϕ_1 on the ratio of limiting stresses.

3.2 Virtual displacement field below the fan

The field below the fan can be conveniently given in terms of the new coordinate system such that the Cartesian coordinates of any given point (α',β') are found from the Cartesian coordinates of the points at the bottom of the fan:

$$x(\alpha',\beta') = \int_0^{\beta'} B(\phi_1-\zeta,\zeta)\mathrm{d}\zeta\,, \quad (18)$$

$$y(\alpha',\beta') = \int_0^{\alpha'} A(\phi_1-\zeta,\zeta)\mathrm{d}\zeta\,, \quad (19)$$

see (4), (5) and Fig. 1. Coordinate β' is equal to the value of ϕ at the point on the bottom of the fan with the same abscissa as the current point, so that $0\leqslant\beta'\leqslant\phi_1$. Similarly, coordinate α' is equal to the angle ϕ at the point on the bottom of the fan with the same ordinate as the current point, so that $0\leqslant\alpha'\leqslant\beta'$. The boundary with the fan is reached when $\alpha'=\beta'$. Lamé coefficients for this coordinate system have a particularly simple form:

$$A' = \sqrt{\left(\frac{\partial x}{\partial\alpha'}\right)^2+\left(\frac{\partial y}{\partial\alpha'}\right)^2} = A(\phi_1-\alpha',\alpha')\,, \quad (20)$$

$$B' = \sqrt{\left(\frac{\partial x}{\partial\beta'}\right)^2+\left(\frac{\partial y}{\partial\beta'}\right)^2} = B(\phi_1-\beta',\beta')\,, \quad (21)$$

(note that the coordinate system within the fan was right-handed and the newly introduced coordinate system is left-handed, hence the rotation below the fan ω' will be of the opposite sign to the rotation within the fan ω).

The solution below the fan features only vertical tension members. The corresponding strain field must have the first principal strain at the maximum allowable limit, whereas the second principal strain $\varepsilon_2'=\varepsilon_2'(\alpha',\beta')$ must remain within the allowable limits. The shearing strain must vanish. These requirements are encapsulated by the following system of partial differential equations for virtual dis-

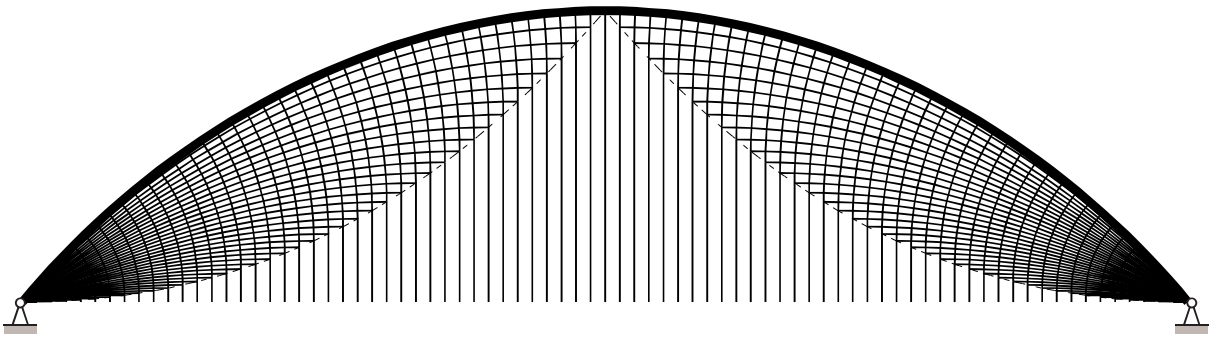

Fig. 4 The discretized optimum structure in the case when $\sigma_T/\sigma_C \approx 0.417785$, i.e. when $h = l/2$.

placements (u', v'):

$$\frac{\partial u'}{\partial \alpha'} = \frac{\ell\sigma}{\sigma_T} A', \quad \omega' = -\frac{1}{B'}\frac{\partial u'}{\partial \beta'}, \tag{22}$$

$$\frac{\partial v'}{\partial \alpha'} = \omega' A', \quad \varepsilon_2' = \frac{1}{B'}\frac{\partial v'}{\partial \beta'}. \tag{23}$$

An equivalent system of partial differential equations was formulated by Hemp (1973, eqn. (4.17)). Also, u' and v' are assumed positive in directions of increasing α' and β' respectively.

In view of equality (20), equation $(22)_1$ can be integrated directly, and the continuity with (11) leads to the following result

$$u' = \ell\sigma y(\alpha', \beta')/\sigma_T - \frac{\ell\sigma l^2}{2h}\left(\frac{1}{\sigma_C} + \frac{1}{\sigma_T}\right)\left(I_0(2\phi_1) - I_0(2\phi_1 - 2\beta')\right), \tag{24}$$

within which we also used equation (4). Since B' is given by (21), it is then straightforward to use $(22)_2$ to establish the rotation

$$\omega' = 2\ell\sigma\left(\frac{1}{\sigma_C} + \frac{1}{\sigma_T}\right)(\phi_1 - \beta'). \tag{25}$$

The integral of equation $(23)_1$, once matched to displacements within the fan, is somewhat more complicated

$$v' = -\ell\sigma x(\alpha', \beta')/\sigma_C + 2\ell\sigma\left(\frac{1}{\sigma_C} + \frac{1}{\sigma_T}\right)\left[\int_0^{\beta'} (\phi_1 - \zeta)A(\phi_1 - \zeta, \zeta)\mathrm{d}\zeta - (\phi_1 - \beta')\int_{\alpha'}^{\beta'} A(\phi_1 - \zeta, \zeta)\mathrm{d}\zeta\right]. \tag{26}$$

Fortunately, we only need this expression to compute the second principal strain from equation $(23)_2$. The result has the form

$$\varepsilon_2' = -\frac{\ell\sigma}{\sigma_C} + 2\ell\sigma\left(\frac{1}{\sigma_C} + \frac{1}{\sigma_T}\right)\frac{\int_{\alpha'}^{\beta'} A(\phi_1 - \zeta, \zeta)\mathrm{d}\zeta}{B(\phi_1 - \beta', \beta')}. \tag{27}$$

It is easily verified that the partial derivative of (27) with respect to α' does not vanish for $0 < \alpha' < \beta'$. This means that the extreme values of ε_2' with respect to α' are reached when $\alpha' = 0$ and/or $\alpha' = \beta'$. In the case when $\alpha' = \beta'$, i.e. at the bottom of the fan, $\varepsilon_2' = -\ell\sigma/\sigma_C$ which is consistent with the requirements of the Michell criteria. Thus, to ensure that the field below the fan satisfies the Michell criteria, we need to verify that

$$-\frac{\ell\sigma}{\sigma_C} \leqslant -\frac{\ell\sigma}{\sigma_C} + 2\ell\sigma\left(\frac{1}{\sigma_C} + \frac{1}{\sigma_T}\right)\frac{y(\phi_1 - \beta', \beta')}{B(\phi_1 - \beta', \beta')} \leqslant \frac{\ell\sigma}{\sigma_T}. \tag{28}$$

First, we note that $y(\phi_1 - \beta', \beta')/B(\phi_1 - \beta', \beta')$ is positive for all $0 \leqslant \beta' \leqslant \phi_1$. Second, it follows from definitions (2) and (5) that $y(\phi_1 - \beta', \beta')$ is a monotonically increasing function of β'. Third, it is evident upon inspection of (3) that $B(\phi_1 - \beta', \beta')$ is a monotonically decreasing function of $0 \leqslant \beta' \leqslant \phi_1$. Therefore, the non-constant term within (28) is growing monotonically as β' increases, and for (28) to be true we only need to ensure that

$$-\frac{\ell\sigma}{\sigma_C} \leqslant -\frac{\ell\sigma}{\sigma_C} + 2\ell\sigma\left(\frac{1}{\sigma_C} + \frac{1}{\sigma_T}\right)\frac{h}{B(0, \phi_1)} \leqslant \frac{\ell\sigma}{\sigma_T}. \tag{29}$$

The inequality on the left is trivial; the inequality on the right may be shown, after referring to equation (3), to indicate that (29), and, consequently, (28), are equivalent to

$$h \leqslant \frac{l}{2}. \tag{30}$$

This essentially constitutes the principal result of this paper, namely that the optimal structure suggested by Hemp's can only satisfy the Michell criteria provided its height is less than or equal to the quarter-span. What does this condition mean in terms of the fan angle and the ratio of limiting stresses? The condition $h = l/2$ is equivalent, see (6), to stating that $\phi_1 \approx 0.878060$. Because of equality (17), the latter condition is equivalent to $\sigma_T/\sigma_C \approx 0.417785$. In addition, we stated at the end of Section 3.1 that h/l and ϕ_1 increase

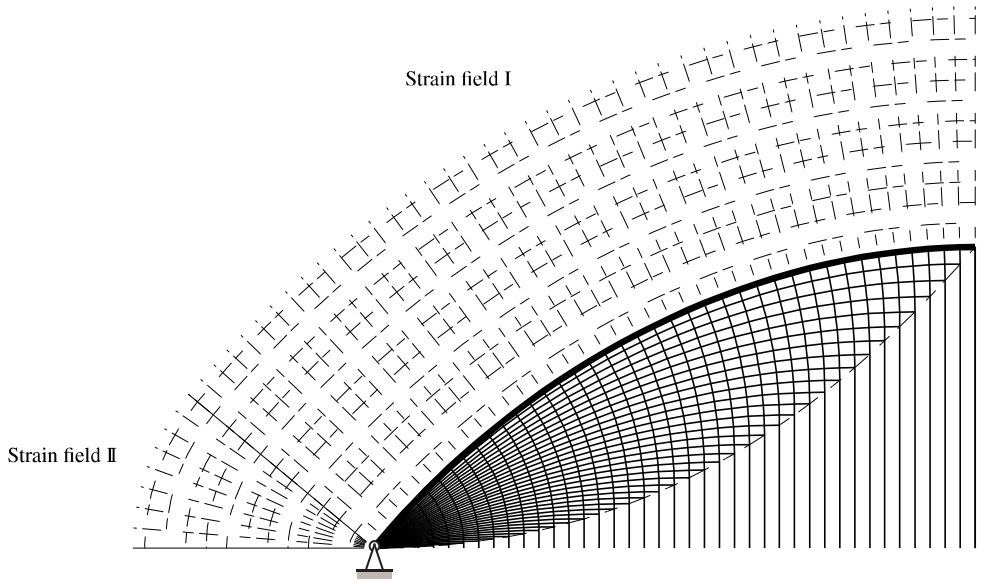

Fig. 5 A sketch of the virtual displacement field covering the entire upper half-plane (shown for the case when $\sigma_T/\sigma_C \approx 0.417785$).

(or decrease) simultaneously with the ratio σ_T/σ_C. Therefore, condition (30) may be equivalently reformulated as

$$\sigma_T/\sigma_C \leqslant 0.417785\,. \tag{31}$$

The discretized version of the tallest Hemp's arch to still satisfy condition (31) is presented in Fig. 4. Let w denote the magnitude (per unit length) of the distributed load. It can then be observed that when $h = l/2$, moment equilibrium at mid-span requires that the compression force in the concentrated top rib of the fan has magnitude wl.

3.3 Proof of optimality for the upper half-plane

The constructed virtual displacement field for the structure satisfies the requirements of the Michell criteria provided (30) (or, equivalently, (31)) is satisfied. Generally speaking, to prove the optimality of the described structure for the upper half-plane, one needs to construct a continuous virtual displacement field that covers the entire upper half-plane. Appendix 4 of Hemp's paper shows how to do this when the limiting stresses are equal and Hemp's argument can easily be applied to the present case, as shown in Fig. 5. The area above the structure can be covered by the strain field 'I' formed by the normals to the concentrated compression bar at the top of the structure. For convenience the coordinate α within this field can be re-defined to represent the distance from the top of the structure, $\alpha \leqslant 0$, while β can remain unchanged, i.e. as within the fan, $0 \leqslant \beta \leqslant \phi_1$. In this case

$$A_{\rm I} = 1\,, \quad B_{\rm I} = B(0,\beta) - \alpha\,, \quad \phi_{\rm I} = -\pi/2 + \phi_1 - \beta\,, \tag{32}$$

and rotation $\omega_{\rm I}$ remains the same as given by equation (7) when $\alpha = 0$. The associated virtual displacement field is given by

$$u_{\rm I} + {\rm i}v_{\rm I} = \ell\sigma\left[\frac{1}{\sigma_T} - {\rm i}\left(\frac{1}{\sigma_C} + \frac{1}{\sigma_T}\right)(\phi_1 - \beta)\right]\alpha$$
$$-\ell\sigma{\rm e}^{{\rm i}\beta}\int_0^\beta {\rm e}^{-{\rm i}\zeta}\left[\frac{\rm i}{\sigma_C} - \left(\frac{1}{\sigma_C} + \frac{1}{\sigma_T}\right)(\phi_1 - \zeta)\right]B(0,\zeta)\,{\rm d}\zeta\,. \tag{33}$$

This field may be shown to match with the field at the top of the fan. It is also worth noting that $v_{\rm I}$ vanishes when $\beta = \phi_1$. Hence, field (33) can be reflected with respect to the vertical line $x = l$ to cover the plane above the right hand side of the structure. The remaining sector of the upper half plane may be covered by a field 'II' consisting of straight lines and circular arcs. Within this field we can conveniently use the same definition of α as adopted within field 'I' but now redefine β to denote the polar angle from the line separating regions 'I' and 'II', $-\pi/2 + \phi_1 \leqslant \beta \leqslant 0$. It is then straightforward to establish that

$$A_{\rm II} = 1\,, \quad B_{\rm II} = -\alpha\,, \quad \phi_{\rm II} = -\pi/2 + \phi_1 - \beta\,. \tag{34}$$

The associated rotation has the form

$$\omega_{\rm II} = -\ell\sigma\left(\frac{1}{\sigma_C} + \frac{1}{\sigma_T}\right)(\phi_1 - \beta)\,, \tag{35}$$

with the corresponding virtual displacement field given by

$$u_{\rm II} + {\rm i}v_{\rm II} = \ell\sigma\left[\frac{1}{\sigma_T} - {\rm i}\left(\frac{1}{\sigma_C} + \frac{1}{\sigma_T}\right)(\phi_1 - \beta)\right]\alpha\,. \tag{36}$$

Fields (33) and (36) clearly match along the line $\beta = 0$. This completes the proof of optimality for the half-plane.

Table 1 Analytical, numerical and extrapolated numerical optimum volumes (expressed in terms of wl^2/σ_C) for various σ_T/σ_C values.

σ_T/σ_C	Exact analytical volume, from (39)	Non-optimal analytical volume, from (39) or [48]	Numerical volume, $n_x = 360$ (diff %)	Extrapolated numerical volume, $n_x = \infty$ (diff %)
0.2	5.58872	—	5.59301 (+0.077%)	5.58917 (+0.008%)
0.3	4.72830	—	4.73136 (+0.065%)	4.72799 (-0.007%)
0.4	4.23346	—	4.23600 (+0.060%)	4.23348 (+0.0005%)
0.417785	4.16607	—	4.16852 (+0.059%)	4.16625 (+0.004%)
1.0	—	3.15548 †	3.15325 (-0.071%)	3.15163 (-0.122%)

† Hemp (1974) reported a non-optimal analytical volume of 3.152 wl^2/σ_C, but his computation was slightly inaccurate. The result presented here is obtained by a more accurate computation of (39) (identical to Hemp's [48] when $\sigma_T/\sigma_C = 1$).

3.4 Volume of the resulting structure

If, once again, w denotes the magnitude per unit length of the distributed load, then the volume of the structure can be determined as the virtual work of the applied load divided by $\ell\sigma$:

$$V_{\min} = \frac{2}{\ell\sigma}\int_0^l -wu'(0,\beta')\mathrm{d}x = \frac{2}{\ell\sigma}\int_0^{\phi_1} -wu'(0,\beta')\frac{\partial x}{\partial \beta'}\mathrm{d}\beta' . \quad (37)$$

By using equations (4), (6), (16), (18) and (24) it is possible to reduce integral (37) to the following expression

$$V_{\min} = \frac{wl^4}{2h^2}\left(\frac{1}{\sigma_C}+\frac{1}{\sigma_T}\right)\left[2I_0(2\phi_1)H_1(\phi_1) - H_2(\phi_1)\right]. \quad (38)$$

The explicit expressions for $H_1(\phi_1)$ and $H_2(\phi_1)$, equation (17), and a small algebraic manipulation can now be used to recast (38) in the compact explicit form

$$V_{\min} = \frac{wl^3}{2h}\left[\left(\frac{1}{\sigma_C}+\frac{1}{\sigma_T}\right)I_0(2\phi_1) - \frac{1}{\sigma_T}\right], \quad (39)$$

which generalizes Hemp's equation [48].

4 Numerical verification

As stated earlier, the present study was partly motivated by the recent availability of high resolution numerical data corresponding to Hemp's arch problem, e.g. as shown in Fig. 2. Therefore, in addition to performing extensive analytical checks (e.g. see Appendix), it is clearly also useful to confirm the new analytical expressions using numerical layout optimization techniques. Thus in Table 1 analytically and numerically determined volumes are presented for various values of σ_T/σ_C.

For cases when $\sigma_T/\sigma_C \leqslant 0.417785$ it is evident from Table 1 that the volumes computed numerically are, as expected, all higher than the corresponding exact analytical volumes. However, the differences are comparatively small (all within 0.1%), and extrapolated numerical volumes as calculated by the method described in Darwich et al (2010) are closer still (all within 0.01%), demonstrating the very good agreement which exists between the analytical and numerical solutions. In the numerical solutions it was also observed that the hangers remained vertical when $\sigma_T/\sigma_C \leqslant 0.417785$, but non-vertical hangers started to emerge as the ratio of limiting tensile to compressive stresses exceeded this threshold value.

For the case when $\sigma_T/\sigma_C = 1.0$ it is evident that the volume computed numerically falls *below* the volume computed using (39) or Hemp's expression [48], providing numerical confirmation of the non-optimal nature of the vertical hanger solution in this case. Given the close correspondence of the other numerical and exact solutions, the extrapolated volume given in Table 1, i.e. $V = 3.15163\ wl^2/\sigma_C$, can be expected to represent a very good approximation of the true optimal volume. This is 0.122% lower than the volume obtained when vertical hangers are assumed.

Note that to obtain the numerical results, the adaptive layout optimization described by Gilbert and Tyas (2003) was used. Nodes were laid out on a rectilinear grid but to facilitate accurate modelling in the flat crown region of the arch, the spacing between nodes in the y direction, Δy, was always taken as half the spacing between nodes in the x direction, Δx (where $\Delta x = 2l/n_x$, where n_x is the number of divisions between nodes in the x direction across the full span, taken as 360 in Table 1). Taking advantage of symmetry but using full connectivity gave rise to models comprising 181×253 nodal points and 1 048 476 528 potential bars. The individual point loads used to approximate the uniformly distributed applied load were taken

to have magnitude $Wn_x/(n_x+1)(n_x-1)$, denoted 'Type-III' in Darwich et al (2010), where in the present study $W = 2wl$. Finally, the extrapolated volumes shown in Table 1 were obtained using the power law extrapolation scheme described in Darwich et al (2010), using models comprising $n_x = 80, 120, 160, \ldots, 360$ divisions to provide source data.

It is worth noting that McConnel (1974) also used an extrapolation approach to estimate the volume of optimal structures of the forms shown in Figures 1 and 2 for an infinite number of point loads. Given the limited computational resources of the day, it is remarkable that his extrapolated predictions for these two cases were within 0.01% of the correct analytical value and the numerical result presented herein. (Volumes of 3.15528 wl^2/σ_C and 3.15148 wl^2/σ_C respectively can be deduced from McConnel's Table 1.)

5 Concluding remarks

It has been demonstrated that the optimal arch structure incorporating vertical hanger bars suggested by Hemp can only satisfy the Michell criteria, and hence be an optimal solution, when its height is less than or equal to the quarter-span. Assuming an upper half-plane design domain, this has been shown to be true when the ratio of limiting tensile to compressive stresses falls below 0.417785.

It is worth noting that the uniformly distributed load problem considered here can also be interpreted as the limiting case for a problem comprising N equally-spaced point loads distributed along the span, as $N \to \infty$ (i.e. $N = n_x + 1$). In particular, the results by McConnel (1974) cited earlier were obtained from numerical solutions featuring from 1 to 19 point loads. Full analytical solutions are presently available for the case when $N = 1$; see Michell (1904), Hemp (1973) and a recent paper by Rozvany and Sokół (2012) who consider the case of unequal limiting stresses. Sokół and Lewiński (2010) recently obtained an analytical solution for the case when $N = 2$, which is valid when $\sigma_C = \sigma_T$).

Finally, although the form of the resulting structure is undeniably complex, it should perhaps be noted that stipulation of a limiting tensile stress which is lower than the limiting compressive stress is potentially reasonable from a practical perspective. This is because materials with good mechanical characteristics in compression (only) are generally much less expensive than those which also have good tensile capacity, and can therefore be used to form compressive elements which are efficient provided adequate restraint against buckling is available.

References

Chan HSY (1975) Symmetric plane frameworks of least weight. In: Sawczuk A, Mŕoz Z (eds) Optimization in Structural Design, Springer, Berlin, pp 313–326

Darwich W, Gilbert M, Tyas A (2010) Optimum structure to carry a uniform load between pinned supports. Structural and Multidisciplinary Optimisation 42(1):33–42

Gilbert M, Tyas A (2003) Layout optimization of large-scale pin-jointed frames. Engineering Computations 20(8):1044–1064

Gilbert M, Darwich W, Tyas A, Shepherd P (2005) Application of large-scale layout optimization techniques in structural engineering practice. In: Proceedings of the Sixth World Congress on Structural and Multidisciplinary Optimization, Rio de Janeiro, Brazil

Hemp WS (1973) Optimum Structures. Clarendon Press, Oxford

Hemp WS (1974) Michell framework for uniform load between fixed supports. Engineering Optimization 1(1):61–69

McConnel RE (1974) Least-weight frameworks for loads across span. Proceedings of the ASME: Journal of Engineering Mechanics Division 100(5):885–901

Michell AGM (1904) The limits of economy of material in frame-structures. Philosophical Magazine 8(47):589–597

Pichugin AV, Tyas A, Gilbert M (2011) Michell structure for a uniform load over multiple spans. In: Proceedings of the Ninth World Congress on Structural and Multidisciplinary Optimization (WCSMO-9), Shizuoka, Japan

Rozvany GIN (1997) Partial relaxation of the orthogonality requirement for classical Michell trusses. Structural and Multidisciplinary Optimization 13(4):271–274

Rozvany GIN, Prager W (1979) A new class of structural optimization problems: optimal archgrids. Computer Methods in Applied Mechanics and Engineering 19(1):127–150

Rozvany GIN, Sokół T (2012) Exact truss topology optimization: allowance for support costs and different permissible stresses in tension and compression — extensions of a classical solution by Michell. Structural and Multidisciplinary Optimization (in press)

Rozvany GIN, Wang CM (1983) On plane Prager-structures—I. International Journal of Mechanical Sciences 25(7):519–527

Rozvany GIN, Bendsøe MP, Kirsch U (1995) Layout optimization of structures. Applied Mechanics Reviews 48(2):41–119

Sokół T (2011) A 99 line code for discretized Michell truss optimization written in Mathematica. Structural and Multidisciplinary Optimization 43(2):181–190

Sokół T, Lewiński T (2010) On the solution of the three forces problem and its application in optimal designing of a class of symmetric plane frameworks of least weight. Structural and Multidisciplinary Optimization 42(6):835–853

Tyas A, Pichugin AV, Gilbert M (2011) Optimum structure to carry a uniform load between pinned supports: exact analytical solution. Proceedings of the Royal Society A 467(2128):1101–1120

Appendix

Various tests can be devised to confirm the correctness of the analytical derivations presented in this paper. One such test involves computing the integral of the horizontal strains along the line joining the supports, at the bottom of the optimum structure, and checking that this equals zero; details of this test follow.

Using the notation of Section 3.2, and referring to equations (18) and (27), the sought for integral can be expressed as the sum of two terms

$$\begin{aligned}\int_0^l \varepsilon_x'|_{y=0}\mathrm{d}x &= \int_0^{\phi_1} \varepsilon_2'|_{\alpha'=0}\frac{\partial x}{\partial \beta'}\,\mathrm{d}\beta' \\ &= 2\ell\sigma\left(\frac{1}{\sigma_C}+\frac{1}{\sigma_T}\right)\int_0^{\phi_1}\int_0^{\beta'} A(\phi_1-\zeta,\zeta)\,\mathrm{d}\zeta\,\mathrm{d}\beta' \\ &\quad -\frac{\ell\sigma}{\sigma_C}\int_0^{\phi_1} B(\phi_1-\beta',\beta')\mathrm{d}\beta'. \end{aligned} \tag{40}$$

Reference to equation (4) immediately indicates that

$$\int_0^{\phi_1} B(\phi_1-\beta',\beta')\mathrm{d}\beta' = x(0,\phi_1) = l\,. \tag{41}$$

The remaining double (in fact, triple, see (2)) integral on the right hand side of equation (40) can be expressed in terms of the already known integral $H_0(\phi_1)$, by changing the order of integration:

$$\begin{aligned}\int_0^{\phi_1}\int_0^{\beta'} A(\phi_1-\zeta,\zeta)\,\mathrm{d}\zeta\,\mathrm{d}\beta' &= \int_0^{\phi_1}\left(\int_\zeta^{\phi_1}\mathrm{d}\beta'\right)A(\phi_1-\zeta,\zeta)\,\mathrm{d}\zeta \\ &= \int_0^{\phi_1}(\phi_1-\zeta)A(\phi_1-\zeta,\zeta)\,\mathrm{d}\zeta = \frac{l^2}{2h}H_0(\phi_1)\,, \end{aligned} \tag{42}$$

see also (14). Equations (41) and (42), when considered in conjunction with identity (15), lead to an immediate conclusion that

$$\int_0^l \varepsilon_x'|_{\alpha'=0}\mathrm{d}x = 2\ell\sigma\left(\frac{1}{\sigma_C}+\frac{1}{\sigma_T}\right)\frac{l^2}{2h}H_0(\phi_1) - \frac{\ell\sigma}{\sigma_C}l = 0\,, \tag{43}$$

which is as should be expected.